


Optimization of ion cyclotron range of frequencies power absorption in low electron density on EAST

Zhengshuyan Wang^{1,2}, Wei Zhang¹, Lunan Liu¹, Yuhao Jiang^{1,2},
Xinjun Zhang¹, Chengming Qin¹, Yaoyao Guo¹, Liuxin Li¹, Sichun Qiu¹,
Huapeng Zhang³, Yongxin Zhu¹, Tao Jin¹ and Zhiping Li¹

¹Institute of Plasma Physics, Hefei Institutes of Physical Science, Chinese Academy of Sciences,
Hefei 23001, PR China

²University of Science and Technology of China, Hefei 230026, PR China

³Department of Plasma Physics and Fusion Engineering, School of Nuclear Science and Technology,
University of Science and Technology of China, Hefei 230026, PR China

Corresponding authors: Wei Zhang, wei.zhang@ipp.ac.cn; Lunan Liu, liulunan@ipp.ac.cn

(Received 14 January 2025; revision received 4 June 2025; accepted 6 June 2025)

The heating effect of electromagnetic waves in ion cyclotron range of frequencies (ICRFs) in magnetic confinement fusion device is different in different plasma conditions. In order to evaluate the ICRF heating effect in different plasma conditions, we conducted a series of experiments and corresponding TRANSP simulations on the EAST tokamak. Both simulation and experimental results show that the effect of ICRF heating is poor at low core electron density. The decrease in electron density changes the left-handed electric field near the resonant layer, resulting in a significant decrease in the power absorbed by the hydrogen fundamental resonance. However, quite a few experiments must be performed in plasma conditions with low electron density. It is necessary to study how to make ICRF heating best in low electron density plasma. Through a series of simulation scans of the parallel refractive index (n_{\parallel}) of the ICRF antenna, it is concluded that the change of the ICRF antenna n_{\parallel} will lead to the change of the left-handed electric field, which will change the fundamental absorption of ICRF power by the hydrogen minority ions. Fully considering the coupling of ion cyclotron wave at the tokamak boundary and the absorption in the plasma core, optimizing the ICRF antenna structure and selecting appropriate parameters such as parallel refractive index, minority ion concentration, resonance layer position, plasma current and core electron temperature can ensure better heating effect in the ICRF heating experiments in the future EAST upgrade. These results have important implications for the enhancement of the auxiliary heating effect of EAST and other tokamaks.

Key words: fusion plasma, plasma heating, plasma simulation

1. Introduction

Ion cyclotron range of frequency (ICRF) heating has been widely used for thermal plasma heating in magnetic confinement fusion devices (Zhang *et al.* 2024). Due to the weakly collisional nature of hot plasmas, ICRF plasma waves, which are known as fast (magnetosonic) waves, are damped in the plasma core primarily through a few non-collisional wave–particle resonant damping mechanisms that affect both ions and electrons (Hillairet 2023). The wave power is damped on one or several thermal species, resulting in an increase of their kinetic energies and the creation of energetic particle populations (Becoulet 1996). Subsequently, these populations contribute to the heating of the plasma through collisional relaxations. The ICRF heating is employed in the majority of contemporary tokamaks and stellarators at a multi-MW level, and is poised to assume a pivotal role in next-generation experiments and fusion reactors (Wilson & Bonoli 2015; Ongena *et al.* 2017; Mertens *et al.* 2019), such as ITER (Lamalle *et al.* 2015), SPARC (Lin *et al.* 2020), TRT (Baev *et al.* 2021), CFETR (Zhang *et al.* 2022), BEST and DEMO (Bobkov *et al.* 2021).

As is shown in figure 1, the ICRF system on EAST uses two antennas which be installed on I & N ports to generate fast waves and couple several megawatts of power with the edge of the plasma, subsequently propagating towards the plasma core (Zhang *et al.* 2023). The fast waves transfer their energy to the resonant ions situated within the ion cyclotron resonance layer. Therefore, it is evident that optimal ICRF coupling and ICRF power absorption are essential for the effective implementation of ICRF heating, which is necessary for attaining high plasma parameters during the long pulses of EAST. The principal techniques for enhancing ICRF coupling on EAST encompass the reduction of parallel wavenumbers within the power spectrum, the local gas puffing to the ICRF antenna, the diminution of the separatrix–antenna distance, the augmentation of core density, the realignment of the divertor strike point and the optimization of ICRF antenna straps (Zhang *et al.* 2024). For improving core power absorption, optimizing ICRF antenna structure, minority ion concentration, resonance layer position (i.e. ICRF frequency) and exploring three-ion heating schemes yield good results (Zhang *et al.* 2024). Among the methods mentioned above, changing the local or global Sheath Quasi-Linear (SOL) density to improve the ICRF coupling, changing the resonance position and minority ion concentration in the high core electron density condition and using three-ion heating scenarios to increase the ICRF power absorption have been investigated in Zhang *et al.* (2024) on EAST. Vast experiments on EAST show that ICRF heating manifests different heating effects in different heating scenarios. In the discussion of this paper, to simplify the expression, low density refers to a core electron density less than or equal to $3 \times 10^{19} \text{ m}^{-3}$, and high density refers to the core electron density higher than $3 \times 10^{19} \text{ m}^{-3}$. In general, the trade off between antenna coupling and core absorption in ICRF heating is always a problem especially in low density conditions. The purpose of studying different electron densities is to find the appropriate plasma and ICRF parameters to achieve good core absorption, in which both coupling and core absorption remain acceptable. This paper is mainly aimed at investigating the differences of ICRF heating effects in different core electron density conditions in the experiments and optimizing ICRF antenna structure (i.e. parallel refractive index n_{\parallel}), minority ion concentration, resonance layer position (i.e. ICRF frequency f_{IC}), core electron temperature and plasma current to ensure better ICRF heating effects for future EAST experiments.

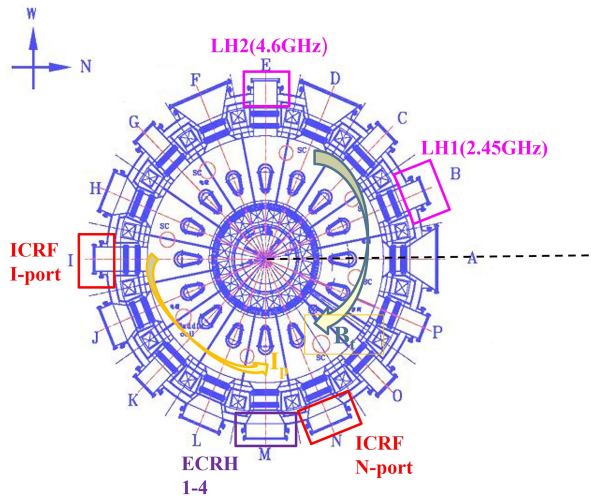


FIGURE 1. Top view of the EAST tokamak with toroidal positions of ICRF, ECRH and LH heating systems used in the experiments in this paper.

2. Comparisons of experiments in high and low core electron densities

EAST is a divertor configuration tokamak with a major radius of $R_0 = 1.85$ m and a minor radius of $a = 0.45$ m. The toroidal distribution of the auxiliary heating systems and neutron diagnostics (Zhong *et al.* 2020) used in the experiments in this paper are shown in figure 1. There are two ICRF antennas, two lower hybrid (LH) antennas and four electron cyclotron resonance heating (ECRH) beams used in the experiments. Two ICRF systems located in the N and I ports have been installed on EAST. The two ICRF antennas are identical, and the ICRF heating frequency is $f_{ICRF} = 37$ MHz, such that the H fundamental (or D second harmonic) resonance position is located at the magnetic axis ($R_0 = 1.85$ m) when toroidal magnetic field $B_t \approx 2.5$ T. All the experiments and simulations discussed in this paper use H minority heating by ICRF with the ICRF antenna phase maintained at 180° .

The left-hand radio-frequency (RF) electric field in figure 2 shows the H fundamental resonance position of experiments in this paper in the poloidal cross-section on EAST computed by TRANSP. In the typical discharge #141913, the ICRF heating effects in high core line integrated electron density n_e was investigated. The general plasma parameters used in this experiment are: toroidal magnetic field $B_t = 2.4$ T, plasma current $I_p = 0.4$ MA, core integrated electron density $n_e = 4 \times 10^{19}$ m $^{-3}$, auxiliary heating power $P_{LH} = 1.8$ MW, $P_{EC} = 2.3$ MW and $P_{IC} = 1$ MW and the core hydrogen concentration is $n(H) = 5\%$. As can be seen from figure 3, time intervals from 6.0 to 8.0 s and 9.0 to 11.0 s with all the three auxiliary heating methods are considered. Because the change in the ICRF power absorption cannot be directly measured, it is indicated by variations in the plasma stored energy, poloidal beta and core plasma temperature. All the plasma conditions are the same except the core line integrated electron density. Figure 4 shows the comparisons of increment of plasma stored energy $WMHD$, neutron yield Yn , core electron temperature T_{e0} and poloidal beta β_p caused by adding ICRF in high and low core line integrated electron density conditions. Comparing with the low core line integrated electron density case #141873, the high core line integrated electron density case #141913 increases the increment of poloidal beta, plasma stored energy, neutron

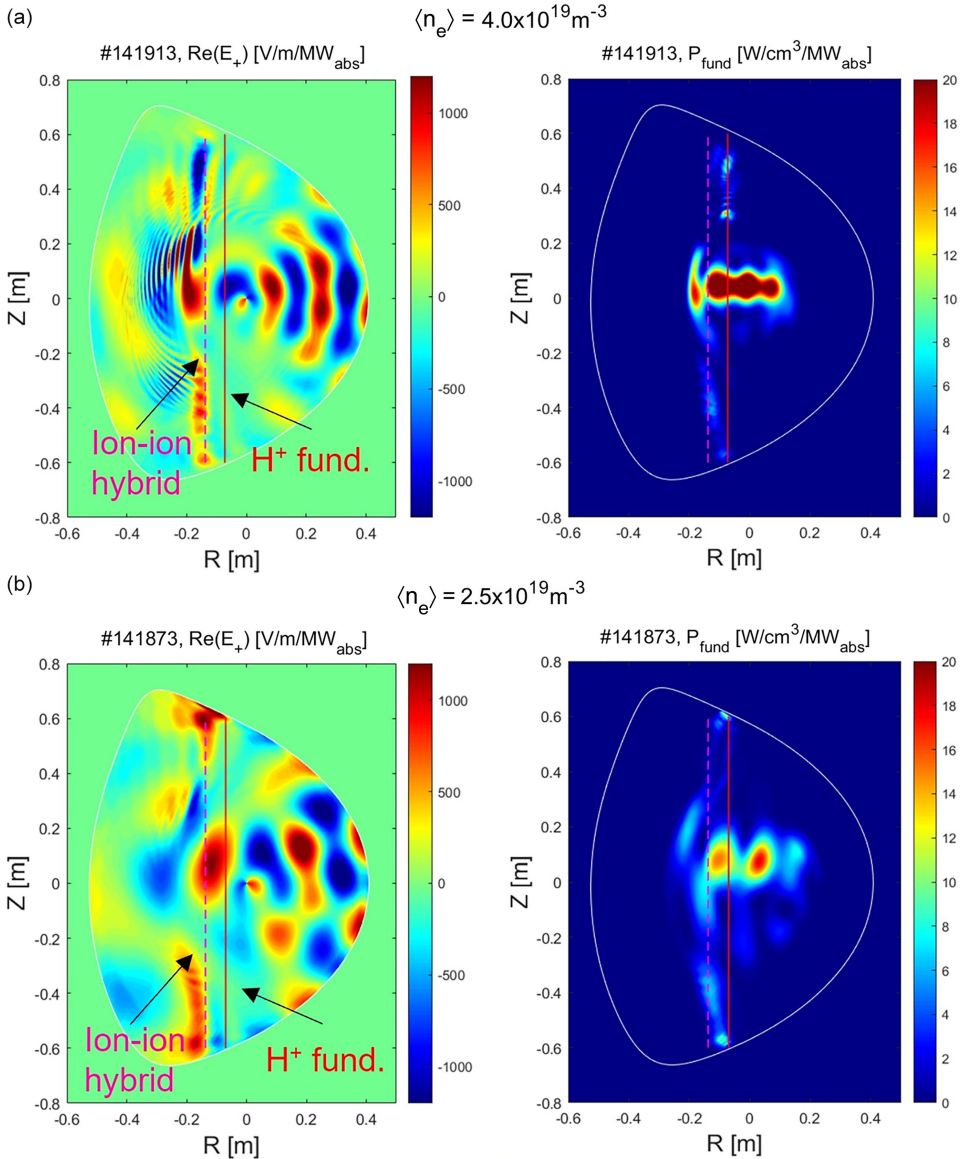


FIGURE 2. The left-hand electric field E_+ and RF power absorbed by H fundamental PF_{fund} for cases with (a) $\langle n_e \rangle = 4.0 \times 10^{19} \text{ m}^{-3}$; (b) $\langle n_e \rangle = 2.5 \times 10^{19} \text{ m}^{-3}$. The red solid line represents the H fundamental or the D second harmonic resonance layer, and the magenta dashed line represents the ion–ion hybrid resonance layer. The unit $\text{MW/m}^{-3}/\text{MW}_{\text{abs}}$ means the RF power absorption density when 1 MW ICRF power is absorbed by the plasma.

yield and electron temperature caused by adding ICRF by 52.31 %, 31.43 %, 50.94 % and 42.31 %, respectively. These phenomena indicate that ICRF heating effects perform better in higher core electron density conditions. The Fokker Planck Package (FPP) (Hammett 1986), coupled to the ICRF full wave deposition code TORIC (Brambilla 1999), is used to interpret these results. More details are discussed in the next section.

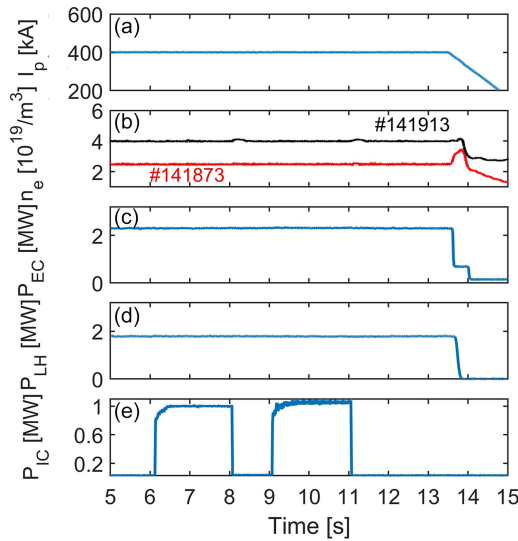


FIGURE 3. Overview of the #141913 and #141873 experimental time traces: (a) plasma current I_p ; (b) core line integrated electron density $\langle n_e \rangle$; (c) ECRH heating power P_{EC} ; (d) LH heating power P_{LH} ; (e) ICRF heating power P_{IC} .

3. Comparative evaluations of ICRF heating effects by TRANSP simulations

In order to help interpret the experiments in § 2, a series of TRANSP simulations (Breslau *et al.* 2018; Pankin *et al.* 2024) have been carried out. The TORIC code (Brambilla 1999) simulates propagation and absorption of the ICRF waves. In the simulations, the magnetic equilibrium, plasma current, loop voltage, toroidal magnetic field, major radius as well as the ion temperature (T_i), electron temperature (T_e) and electron density (n_e) profiles were used as inputs. The ion density is determined by the ion compositions and charge conservation. Figure 5 shows the two-dimensional profiles n_e , T_e and T_i at 10.0 s varying with the toroidal normalized grid ρ_{tor} used as inputs in the simulations. In addition, the heating power of ICRF, LH and ECRH were set as the same as the experimental conditions of the cases #141913 and #141873. The Z_{eff} line integrated signal $Z_{eff} = 2.0$ is provided by visible spectroscopy (bremsstrahlung) (Chen *et al.* 2013) along a vertical line of sight as one of the simulation inputs.

Therefore, a set of TRANSP (Pankin *et al.* 2024) simulations was performed to quantify the influence of different core electron densities on the RF power absorption. In the simulations, all the plasma parameters were the same, except for the electron density and electron temperature profiles. The minority ion concentration was set to 5% and the minority H ion heating was the dominant heating scenario. The absorbed ICRF power densities of each plasma species for different core electron densities are shown in figure 6. Noticeably, the absorbed ICRF power density is larger for the high electron density condition relating to a better ICRF heating effect.

The calculated left-hand RF electric field (E_+) and RF power absorption by H minority ions are shown in figure 2. Compare figure 2(a) with figure 2(b), the left-hand RF electric fields (E_+) are different in the region close to the H fundamental (or D second harmonic) resonance layer, leading to different RF power absorptions

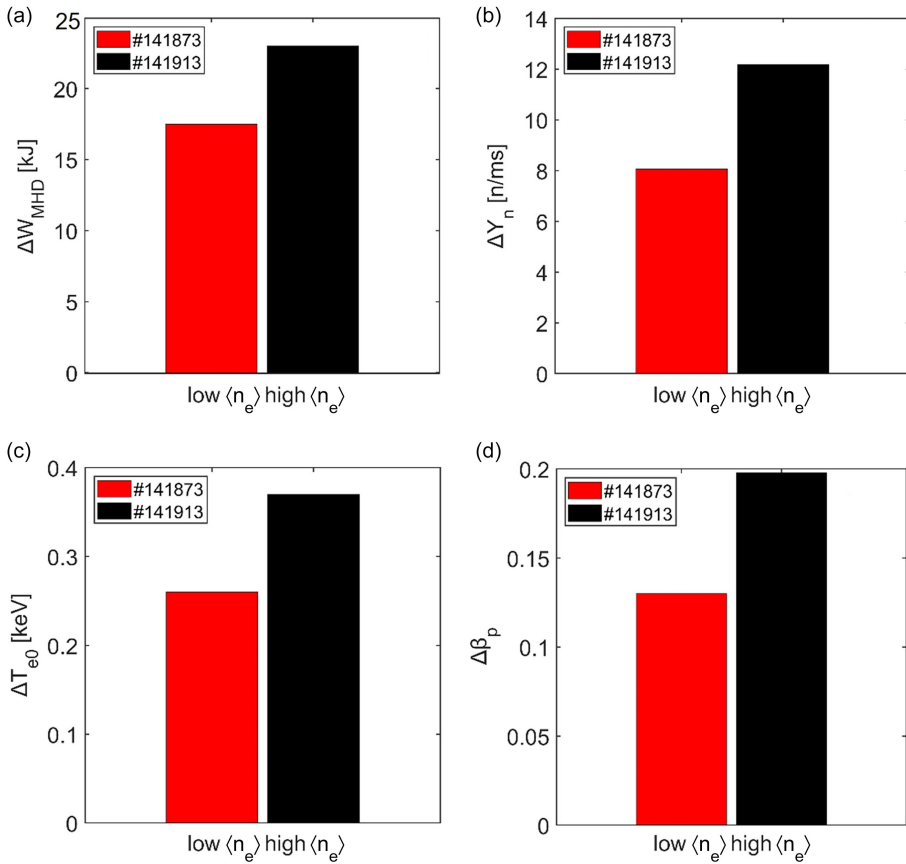


FIGURE 4. Comparisons of increment of (a) plasma stored energy W_{MHD} ; (b) neutron yield Y_n ; (c) core electron temperature T_{e0} and (d) poloidal beta β_p caused by adding ICRF in high and low core line integrated electron density.

by the resonant ions. The RF power absorption density at low electron density is 49.2% lower than that at high electron density. The comparison and evaluation of the above simulation results show that the ICRF heating effect is worse at low core electron density than at high core electron density, which is also consistent with the experimental results in § 2. In order to obtain a better ICRF heating effect, a relatively high core electron density can be selected in the subsequent EAST experiments. More simulations for core electron density have been carried out and related results can be seen in red solid line of figure 8. All the results shown in this section indicate that the ICRF heating effect performs better in high core electron density with the range of $4 \times 10^{19} - 5 \times 10^{19} \text{ m}^{-3}$.

4. Optimizing ICRF core heating effects

4.1. Changing the plasma current

It is clear that the ICRF heating effect performs better in high core electron density conditions. However, there are still plenty of experiments which need to be carried out in low core electron density conditions in the EAST tokamak. In

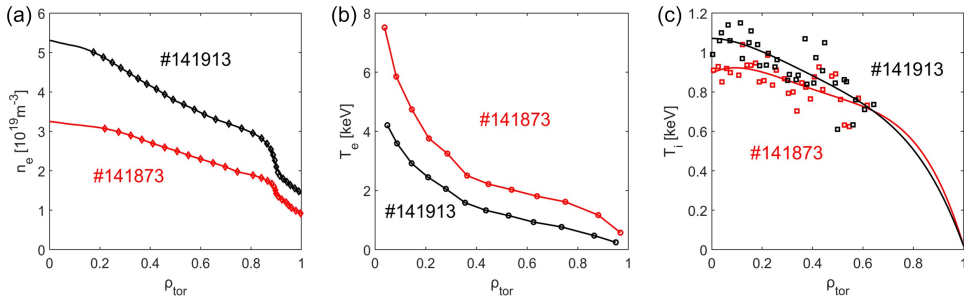


FIGURE 5. The (a) electron density, (b) electron temperature and (c) ion temperature profiles of two cases (high n_e and low n_e) at 10.0 s used as inputs in the TRANSP simulations.

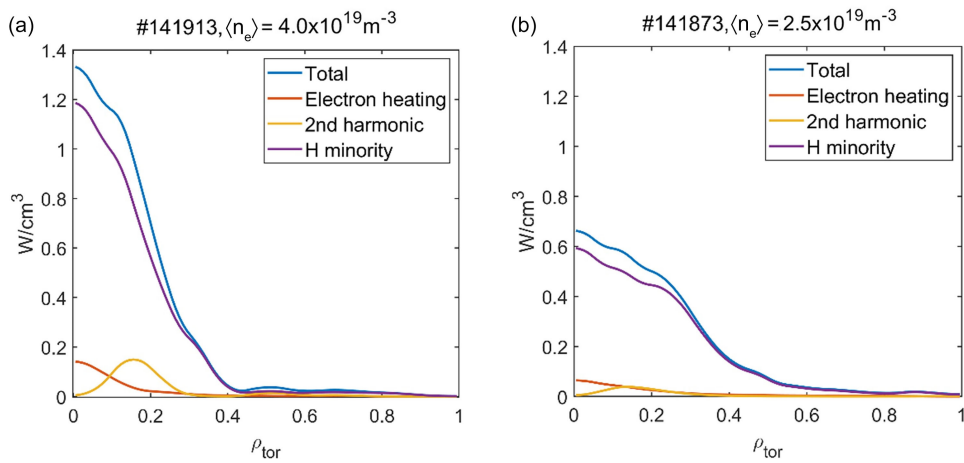


FIGURE 6. Absorbed ICRF power density in (a) high n_e and (b) low n_e plasma conditions.

this case, a series of simulations with plasma parameter scan have been carried out at low core electron density $n_{e0} = 3 \times 10^{19} \text{m}^{-3}$. In this section, the plasma current has been scanned in the low core electron density condition. The ICRF power absorption has been computed by TRANSP (Pankin *et al.* 2024) with the TORIC (Brambilla 1999) and FPP (Hammett 1986) code packages. The electron density, electron temperature and ion temperature profiles are used as the inputs of the simulations using the profiles of discharge #141873, which are shown in figure 4(a–c). The toroidal magnetic field used as input is $B_t = 2.4 \text{ T}$, and the core hydrogen concentration is $n(H) = 5\%$. The plasma current has been changed from 200 to 500 kA. We computed the ICRF absorbed power density of each plasma species for different plasma currents in each cases, and the ratio of ICRF power absorbed by H minority ions over the total ICRF power has also been computed by TORIC, as can be seen in the black solid line in figure 8. Results in 7 and 8 show that the impact of plasma current on ICRF heating effects is not very large. In normal circumstances, the value range studied in this paper is optional for plasma current in the experiments on EAST. In other words, plasma current with the range of 200–500 kA can be seen as a good choice for good ICRF heating effect on EAST.

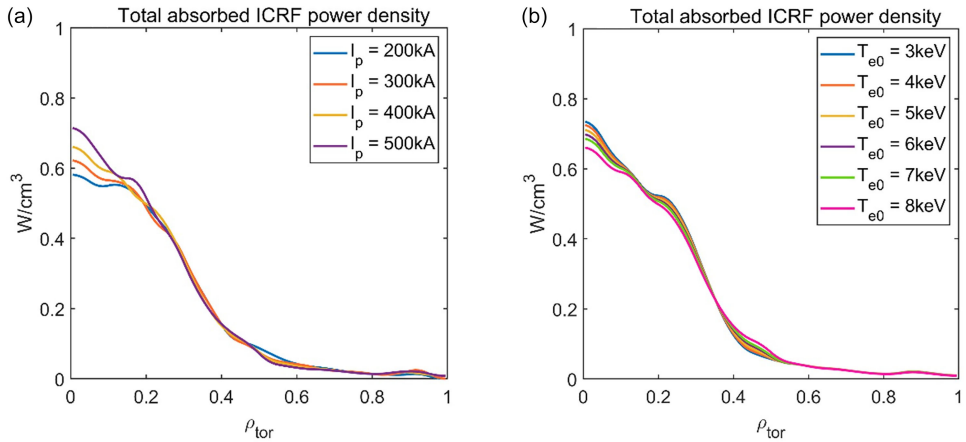


FIGURE 7. Comparisons of total absorbed ICRF power density for cases with (a) different plasma currents and (b) different core electron temperatures.

4.2. Changing the core electron temperature

The simulations in this section are similar to the operations in the previous § 4.1. In this section, core electron temperature has been scanned in the low core electron density condition. The ICRF power absorption has been computed by TRANSP (Pankin *et al.* 2024) with the TORIC (Brambilla 1999) and FPP (Hammett 1986) code packages. The plasma current is $I_p = 400$ kA. The electron density and ion temperature profiles are used as the inputs of the simulations using the profiles of discharge #141873, which are shown in figure 5(a, c). The toroidal magnetic field used as input is $B_t = 2.4$ T, and the core hydrogen concentration is $n(\text{H}) = 5\%$. The core electron temperature has been changed from 3 to 8 keV. We computed the ICRF absorbed power density of each plasma species for different plasma currents in each case, and the ratio of ICRF power absorbed by H minority ions over the total ICRF power has also been computed by TORIC, as can be seen in the blue solid line in figure 8. Results in figures 7 and 8 show that the impact of the core electron temperature on ICRF heating effects is not very large. In normal circumstances, the value range studied in this paper is optional for core electron temperature in the experiments on EAST. In other words, the core electron temperature with the range of 3–8 keV can be seen as a good choice for good ICRF heating effect on EAST.

4.3. Changing parallel refractive index of ICRF antennas

Most of the experiments use an ICRF antenna phase equal to 180° on EAST, this section tends to explore the effect of changing the parallel refractive index n_{\parallel} (i.e. the structure of the ICRF antenna) on the ICRF heating effect, which also provides reference for the reconstruction and upgrading of ICRF antennas on EAST.

A series of simulations by TRANSP (Pankin *et al.* 2024) have been carried out correspondingly. All the simulations use the same parameters as inputs except the parallel refractive index n_{\parallel} . The plasma current is $I_p = 400$ kA. The electron density, electron temperature and ion temperature profiles as the inputs of the simulations used the profiles of discharge #141873, which are shown in figure 5(a–c). The toroidal magnetic field is $B_t = 2.4$ T. The minority ion concentration was set to 5%

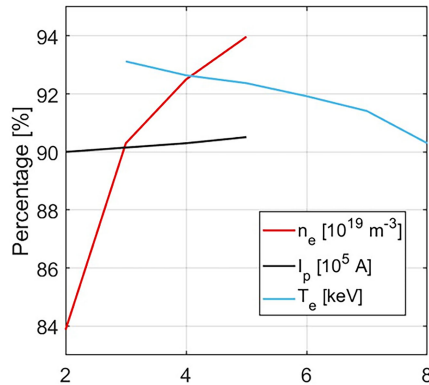


FIGURE 8. The ratio of ICRF power absorbed by H minority ions over the total ICRF power varying with plasma current I_p , core electron density n_{e0} and core electron temperature T_{e0} . Among them, the x axis represents to plasma current I_p [10^5 A], core electron density n_{e0} [10^{19} m⁻³] and core electron temperature T_{e0} [keV].

and the minority H ion heating was the dominant heating scenario. The absorbed ICRF power density for $n// = 10$ – 28 has been computed and one of them is shown in figure 9. The absorbed ICRF power density increases first and then oscillates as $n//$ increases. The left-hand electric field E_+ and ICRF power absorption density with $n// = 10$ – 28 have been computed in the simulations, indicating that the left-hand electric field changes and leading the ICRF power absorption density changes at the H fundamental resonance layer. The ratio of ICRF power absorbed by H minority ions over the total ICRF power varying with $n//$ was computed by TORIC and is shown in figure 10(a). This manifests that the plasma core absorbs the most ICRF power at $n// = 26$, and the absorbed ICRF power is relatively high when $n//$ is larger than 16. As a first approximation, the coupled ICRF power is proportional to the coupling resistance (R_c) for a fixed transmission-line antinode voltage and characteristic impedance. However, the coupling resistance is exponentially related to the parallel wavenumber of the power spectrum ($k//$) and width of the fast wave evanescent layer (d_{evan}), i.e. (Bilato *et al.* 2005; Jacquet *et al.* 2012). Zhang *et al.* (2024) and Hua *et al.* (2024) show that the ICRF coupling power decreases as $n//$ increases.

Figure 10(b) shows the relationship between the coupling resistance (R_c) and the parallel refractive index $n//$. The results in figure 10(b) have been obtained by changing the distance between the two straps and computing the antenna coupling resistance in COMSOL (Tierens *et al.* 2019). Figure 10(b) also indicates that the coupled ICRF power is relatively high when $n//$ is smaller than 20. It is worth mentioning that this is a relative result, as the coupling resistance (R_c) depends on many more parameters than the parallel refractive index $n//$ alone. The ICRF power absorption and coupling are relatively large with the range of $n//$ from 16 to 20. This parallel refractive index $n//$ value range can also obtain a good heating effect in high electron density conditions, as mentioned in Zhang *et al.* (2024) and Hua *et al.* (2024). Thus, the appropriate $n//$ should be chosen within the area including $n//$ with 16–20 as this is more appropriate for better ICRF heating effects considering both the absorbed ICRF power in the plasma core and the coupled ICRF power at the boundary of the plasma.

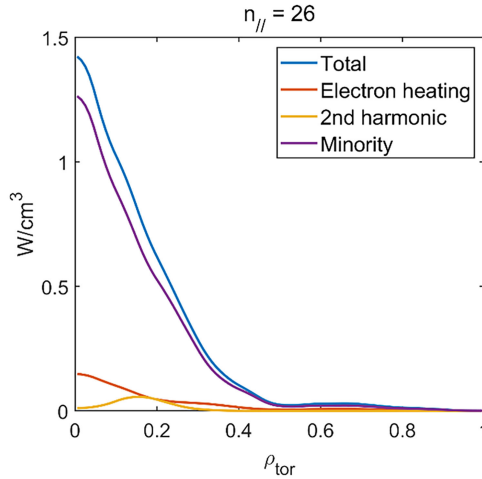


FIGURE 9. Absorbed ICRF power density of each plasma species for parallel refractive index $n_{\parallel} = 26$.

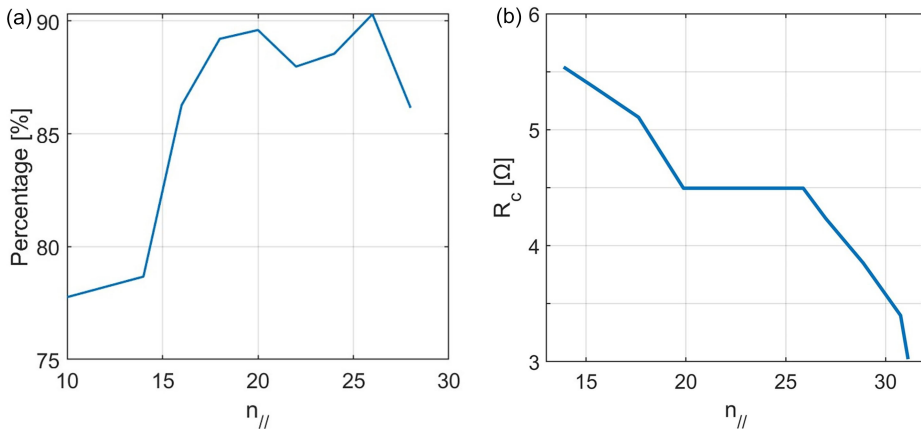


FIGURE 10. (a) The ratio of ICRF power absorbed by H minority ions over the total ICRF power varying with parallel refractive index n_{\parallel} ; (b) coupling resistance (R_c) varying with parallel refractive index n_{\parallel} .

4.4. Changing minority ion concentration

Minority ion concentration is also an important factor that influences the absorbed ICRF power density in the plasma core. It has been investigated from experiments that the highest electron temperature and core heating efficiency were achieved when the edge minority ion concentration $n(\text{H})$ was 10% on EAST (Zhang *et al.* 2024). The value of $n(\text{H})$ at the edge plasma is measured using divertor visible spectroscopy, whereas its value in the plasma core is unknown because of a lack of related diagnostics on EAST. Edge $n(\text{H})$ is expected to be larger than core $n(\text{H})$ because the first wall is the main source of H ions. TRANSP (Pankin *et al.* 2024) simulations are used to scan the core $n(\text{H})$ from 1% to 15% to explore the most appropriate core $n(\text{H})$ for the higher absorbed ICRF power density and better ICRF heating

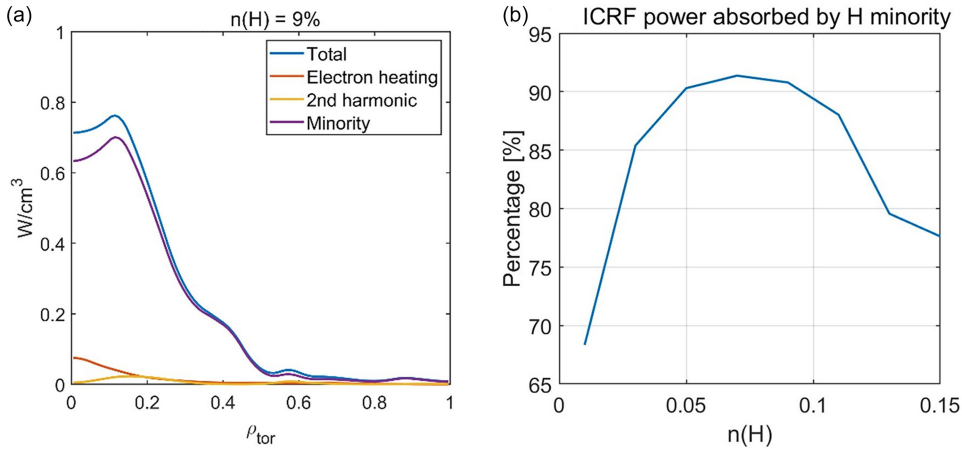


FIGURE 11. (a) Absorbed ICRF power density of each plasma species for hydrogen concentration $n(H) = 9\%$. (b) The ratio of ICRF power absorbed by H minority ions over the total ICRF power varying with hydrogen concentrations.

effects at low core electron density. All the plasma parameters used as inputs for these simulations are the same except the core $n(H)$. The plasma current is $I_p = 400$ kA. The electron density, electron temperature and ion temperature profiles that are used as the inputs of the simulations used the profiles of discharge #141873, which are shown in figure 5(a–c). The toroidal magnetic field is $B_t = 2.4$ T. One of the computed absorbed ICRF power density profiles in these simulations is shown in figure 11(a), including the ICRF power density absorbed by total plasma species, electron heating, deuterium second harmonic heating and the H minority heating. The ICRF absorbed power remains at a relatively high level when the core $n(H)$ is in the 5%–10% area. This is consistent with the theory and conclusions obtained for previous studies at high core electron density on EAST (Zhang *et al.* 2024) and other tokamaks (Wesson & Campbell 2011). Figure 11(b) shows the ratio of ICRF power absorbed by H minority ions over the total ICRF power varying with hydrogen concentrations. It indicates that 5–10% should be an appropriate range of core $n(H)$ for better ICRF heating effects in the experiments in low electron density conditions on EAST.

4.5. Changing ICRF frequency

The positions of the cyclotron resonance layer can be estimated with

$$R = R_0 \frac{q_i B_t}{2\pi f m_i}. \quad (4.1)$$

For a fixed toroidal magnetic field, the ICRF frequency (f_{IC}) determines the H fundamental and D second harmonic resonance position and influences ICRF absorbed power. On EAST, the H fundamental and the D second harmonic resonance position is near the magnetic axis when $f_{IC} = 37$ MHz. Thus, the range $f_{IC} = 31$ –41 MHz was scanned at low core electron density in the TRANSP (Lin *et al.* 2020) simulations. In the simulations, all the plasma parameters were the same, except for the ICRF frequency. The plasma current is $I_p = 400$ kA. The electron density, electron temperature and ion temperature profiles used as the inputs of the simulations used

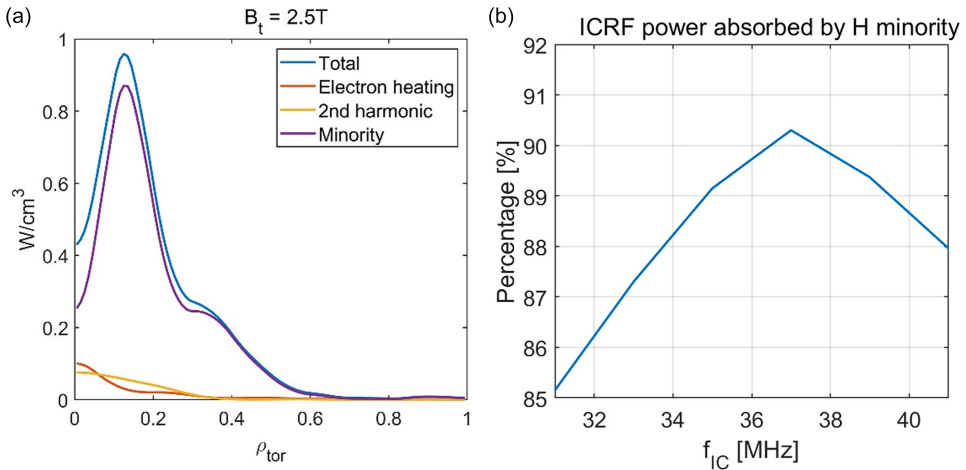


FIGURE 12. (a) Absorbed ICRF power density of each plasma species for ICRF frequency $f_{IC} = 35$ MHz. (b) The ratio of ICRF power absorbed by H minority ions over the total ICRF power varying with ICRF frequency.

the profiles of discharge #141873, which are shown in figure 5(a)–(c). The minority ion concentration was set to 5% and the minority H ion heating was the dominant heating scenario. The toroidal magnetic field was $B_t = 2.4$ T. The computed left-hand electric fields show that the resonance position will move towards the low field side when decreasing f_{IC} , and to the high field side when increasing f_{IC} . Noticeably, the ICRF power absorbed by H minority ions is largest for f_{IC} around 37 MHz and decreases as the resonance layer moves away from the magnetic axis. Figure 12(b) shows that the ratio of ICRF power absorbed by H minority ions over the total ICRF power is relatively large with the range of $f_{IC} = 35$ –39 MHz. This is because, for on-axis heating on EAST, the left-hand electric field (E_+) is relatively large in a region close to the H fundamental (or D second harmonic) resonance layer, leading to the larger ICRF power absorption by the resonant ions. As the resonance layer moves away from the magnetic axis, E_+ close to the resonance layer becomes less significant, leading to a decrease of ICRF power absorption. The ICRF heating effect also performs better when the resonance layer is near the magnetic axis in the high core electron density condition, as mentioned in Zhang *et al.* (2024). This also proves that this value range of ICRF frequency f_{IC} is universal for a better ICRF heating effect in most of the experiments on EAST.

As a consequence, it was demonstrated that the absorption of ICRF power is at its maximum when the resonance position coincides with the magnetic axis (i.e. on-axis heating) or when the hydrogen minority ion concentration at the plasma core is approximately 5%–10% at low electron density. One can also conclude that the ICRF heating effect performs better when the parallel refractive index is between 16 and 20. Plasma current and core electron temperature have little influence on ICRF power absorption within the studied scope of this paper. The range between the blue solid line and the orange solid line in figure 13 represents the five plasma parameter ranges corresponding to a better ICRF heating effect. In the subsequent ICRF-related experiments and even in the upgrading of EAST, the relevant plasma

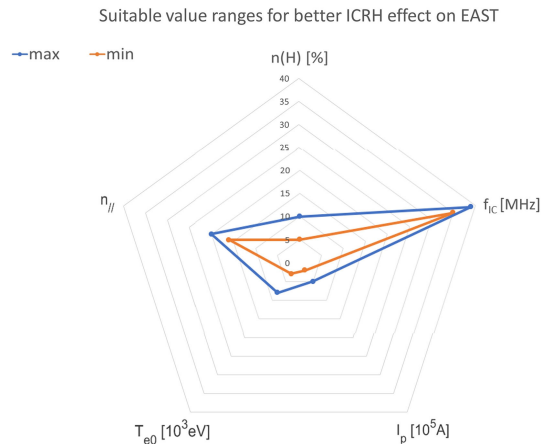


FIGURE 13. Suitable plasma parameter range for better ICRF heating effect in the low core electron density condition on EAST. Among them, the blue solid line represents the maximum value of each plasma parameters for better heating effects, and the orange solid line represents the minimum value of each plasma parameters for better heating effects.

parameters of the conclusions in this paper will be considered to obtain better heating effects and thus better experimental results for experiments in low core electron density conditions.

5. Conclusions

The ICRF heating effect is regarded as a prospective heating methodology for prospective fusion reactors. Therefore, research on improving the ICRF heating effect in this paper is of great significance for future fusion reactor devices. Good ICRF coupling and RF power absorption are both necessary for efficient ICRF heating. This paper mainly focuses on improving the core ICRF power absorption from two aspects of both experiments and simulations to improve the ICRF heating effect.

Parameter scans of the parallel refractive index, minority ion concentration, resonance layer position, plasma current and core electron temperature are performed to increase the core wave power absorption by thermal plasmas in low core electron density conditions. The balancing of ICRF coupling and core ICRF power absorption have been considered in the appropriate parallel refractive index selection in this paper. It is shown in the above investigation that, when the parallel refractive index is between 16 and 20, the ICRF heating effect is better. It is also demonstrated that, when the hydrogen minority ion concentration at the plasma core is approximately 5%–10% or when the resonance position overlaps the magnetic axis (i.e. on-axis heating), the ICRF power absorption is relatively high, resulting in better ICRF heating effects in low core electron density conditions. It is concluded that, within the studied scope of the plasma current and the core electron temperature, the ICRF power absorption changes a little and is always in a good range. The above plasma parameter value ranges are suitable for a better ICRF heating effect on EAST.

This paper not only evaluates ICRF heating effects at different core electron densities in both experiments and simulations, but also presents simulations for different

plasma parameters. The investigations on different ICRF heating scenarios provide important references for experiments on EAST in the future. The simulations about the parallel refractive index are of great significance for the EAST upgrade in the future.

Acknowledgements

This work was supported by National magnetic confinement fusion energy development research project under Grant Nos. 2022YFE03190200 and 2019YFE03070000, by National Natural Science Foundation of China under Grant Nos. 12175273, 12105184, 11975265 and by the Comprehensive Research Facility for Fusion Technology Program of China under Contract No. 2018-000052-73-01001228.

Editor Won Ho Choe thanks the referees for their advice in evaluating this article.

Declaration of interests

The authors report no conflict of interest.

REFERENCES

- BAEV, V.M., GETMAN, D.V., GUBIN, A.M. & SUBBOTIN, M.L. 2021 System of ICR heating of the plasma at the TRT tokamak. *Plasma Phys. Rep.* **47**, 1169–1175.
- BECOULET, A. 1996 Heating and current drive regimes in the ion cyclotron range of frequency. *Plasma Phys. Contr. F.* **38**, A1–A11.
- BILATO, R., BRAMBILLA, M., HARTMANN, D.A. & PARISOT, A. 2005 Influence of an evanescence layer in front of the antenna on the coupling efficiency of ion cyclotron waves. *Nucl. Fusion* **45**, L5–L7.
- BOBKOV, V., *et al.* 2021 Development of pre-conceptual iter-type ICRF antenna design for demo. *Nucl. Fusion* **61**, 046039.
- BRAMBILLA, M. 1999 Numerical simulation of ion cyclotron waves in tokamak plasmas. *Plasma Phys. Contr. F.* **41**, 1–34.
- BRESLAU, J., GORELENKOVA, M., POLI, F., SACHDEV, J., PANKIN, A. & PERUMPILLY, G. 2018 (*usdoe office of science (sc) fusion energy sciences (fes)(sc-24)*). TRANSP Comput. Softw.
- CHEN, Y., WU, Z., GAO, W., ZHANG, L. & ZHA, W. 2013 Z_{eff} first measurements in east with a multi-channel visible bremsstrahlung new system. *Fusion Engng Des.* **88**, 2825–2829.
- HAMMETT, G.W. 1986 Fast ion studies of ion cyclotron heating in the plt tokamak *PhD thesis*. Citeseer.
- HILLAIRET, J. 2023 Review on recent progress in ion cyclotron range of frequency systems, experiments and modelling for magnetic confinement fusion. *Rev. Modern Plasma Phys.* **7**, 16.
- HUA, Y.A., ZHANG, X., SHUAI, Y.U., CHENGMING, Q.I., ZHANG, W., URBANCZYK, G., QIAN, J., LUNAN, L.I., GAOXIANG, W.A. & CHEN, Q. 2024 Physical design and recent experimental results of the new icrf antenna on east. *Plasma Sci. Technol.* **26**, 065601.
- JACQUET, P., *et al.* 2012 Improvement of icrf antenna loading by local gas injection on asdex upgrade. *Nucl. Fusion* **52**, 042002.
- LAMALLE, P., *et al.* 2015 Status of the iter ion cyclotron heating and current drive system. In *AIP Conference Proceedings*, vol. 1689. AIP Publishing.
- LIN, Y., WRIGHT, J.C. & WUKITCH, S.J. 2020 Physics basis for the ICRF system of the sparc tokamak. *J. Plasma Phys.* **86**, 865860506.
- MERTENS, M.A., AERTS, A., INFANTE, I., NEUHAUSEN, J. & COTTENIER, S. 2019 Po-containing molecules in fusion and fission reactors. *J. Phys. Chem. Lett.* **10**, 2879–2884.
- ONGENA, J., *et al.* 2017 Recent advances in physics and technology of ion cyclotron resonance heating in view of future fusion reactors. *Plasma Phys. Contr. F.* **59**, 054002.

- PANKIN, A.Y., BRESLAU, J., GORELENKOVA, M., ANDRE, R., GRIERSON, B., SACHDEV, J., GOLIYAD, M. & PERUMPILLY, G. 2024 Transp integrated modeling code for interpretive and predictive analysis of tokamak plasmas. arXiv: [2406.07781](https://arxiv.org/abs/2406.07781).
- TIERENS, W., *et al.* 2019 Validation of the icrf antenna coupling code raplicasol against topica and experiments. *Nucl. Fusion* **59**, 046001.
- WESSON, J. & CAMPBELL, D.J. 2011, *Tokamaks*, vol. 149. Oxford University Press.
- WILSON, J.R. & BONOLI, P.T. 2015 Progress on ion cyclotron range of frequencies heating physics and technology in support of the international tokamak experimental reactor. *Phys. Plasmas* **22**.
- ZHANG, W., *et al.* 2022 Conceptual design and optimization of an ITER-type ICRF antenna on CFETR. *Nucl. Fusion* **62**, 076045.
- ZHANG, W., *et al.* 2023 Influence of icrf-nbi synergy on fast ion distribution and plasma performance in second harmonic heating experiments with deuterium NBI at east. *Nucl. Fusion* **63**, 056015.
- ZHANG, W., LIU, L., ZHANG, X., QIN, C. & YANG, H. 2024 Recent progress in improvement in ion cyclotron range of frequencies coupling and power absorption with new antennas of experimental advanced superconducting tokamak (east). *Nucl. Fusion* **64**, 096011.
- ZHONG, G., *et al.* 2020 Development of a wide-range neutron flux monitoring system in east. *J. Instrum.* **15**, P05011–P05011.